Effect of Fuel Composition and EGR on Spark-ignited Engine Combustion with LPG Fueling: Experimental and Numerical Investigation

Tanmay Kar[1,2], Toluwalase Fosudo[1], Anthony Marchese[1], Bret Windom[1], and Daniel Olsen[1]

[1]Department of Mechanical Engineering, Colorado State University

[2]Clean Combustion Research Center, King Abdullah University of Science and Technology (KAUST)

Abstract

This paper presents an experimental and numerical investigation of a spark-ignited (SI) cooperative fuel research (CFR) engine fueled with different liquefied petroleum gas (LPG) fuels and exhaust gas recirculation (EGR). The effects of LPG fuel composition on engine combustion characteristics are initially evaluated at two different compression ratios (CR). Results show normal combustion at CR 7 and heavy knocking combustion at CR 10 for all the tested fuels, with a more substantial impact for the LPG fuel with high proportions of n-butane species. The Livengood-Wu (LW) integral method is then used to analyze the knock occurrence risk of individual fuels based on the reactivity of the tested fuels. The introduction of EGR then demonstrates the potential of knock intensity reduction below the borderline knock limit. A zonal-based kinetic interactions study is also performed to understand the knock mitigation effectiveness of EGR over the pressure-temperature domain relevant to SI engine operation. Finally, a multidimensional, computational fluid dynamics (CFD) simulation model is shown to predict the LPG combustion characteristics and presents the evolution of in-cylinder temperature and chemical species to demonstrate the development of end-gas autoignition events without and with EGR.

Keywords

Liquefied petroleum gas, Knock, Exhaust gas recirculation, Ignition delay, Livengood-Wu integral, CFD.

1 Introduction

Over the past decade, research on lower carbon intensity alternative fuels has made significant progress as the demand for efficient and cleaner internal combustion engine operation intensifies [1]. There are several works involving spark-ignited (SI) engines using alternative fuels, which include compressed natural gas [2], liquefied petroleum gas [3], hydrogen [4], and alcohol fuels (methanol and ethanol) [5]. Liquefied petroleum gas (LPG) has emerged as one promising alternative fuel for SI engines, particularly for heavy-duty vehicle applications, due to its high knock resistance [6], easy liquefication capability at relatively low pressure, and lower fuel cost [3]. The composition of LPG fuel primarily consists of propane, n-butane, isobutane, ethane, propene, and butene, with small amounts of methane and other C4-C5 hydrocarbons. LPG is generally extracted from streams of natural gas from oil and gas fields, or obtained as a co-product of refining of crude oil at refineries (which is primarily responsible for the presence of olefins in the LPG fuel) [7]. The proportion of species in LPG fuels varies significantly depending on the extraction region, season, processing method, etc. Its composition also differs considerably from one country to another when used as an automotive fuel, with propane concentration from virtually 100% to as low as 50% [8–11].

Several experimental works [12–14] reported a comparable engine performance and substantial emission benefits with LPG fueling than gasoline. The previous study by the authors [9] demonstrated the impact of LPG composition on the performance and emission behavior of a spark-ignited CFR engine and found similar engine performance with the tested

LPG blends. Ravi et al. [15] demonstrated an improvement in LPG-fueled lean burn SI engine performance and combustion characteristics with higher piston squish area using 3D CFD simulations. Chiriac et al. [16] found higher torque and equal fuel conversion efficiency (at full load) with an optimized LPG-fueled engine compared to the original diesel version of the engine. Campbell et al. [17] showed that the principal LPG fuel constituents (i.e., propane, n-butane, and iso-butane) have similar burn rates when used as SI engine fuels. Furthermore, compared to gasoline, propane fueling requires more spark advance at low engine speed while less advancement at high speed [18].

The performance of an LPG-fueled SI engine is shown to be improved with the increase of compression ratio [8,19], but the onset of knock may restrict the upper limit of CR. Knock is generally defined as the mechanical response of the engine to non-uniform pressure distribution in the combustion chamber. This occurs as a result of the abnormally high rate of heat release due to autoignition of the end-gas ahead of the propagating flame front [20]. For hydrocarbons, the pre-flame chemical oxidation reactions being exothermic in nature heat up the end-gas, which may lead to autoignition and thereby engine knock. The knock resistance of a conventional SI engine fuel is generally characterized by two octane numbers - the Research Octane Number (RON) [21] and the Motor Octane Number (MON) [22]. Smith et al. [23] found that the end-gas autoignition of major LPG fuel species (i.e., propane, butane) is dominated by the intermediate and high-temperature reactions and by the amount of time the end gas spends at temperatures above approximately 900 K. Ramalingam et al. [24] studied the oxidation behavior of four different LPG blends (as per the mixture requirement of EN 589) at stoichiometric 20 bar conditions and found changes in the reactivities of the fuels in the low-to-intermediate temperature regimes. A knock limit study in a gas-fueled SI engine by Badr et al. [25] showed a much lower knocking limit of LPG than that with propane due to the higher reactivity of LPG. For pure propane and commercial LPG fuels, the

end gas also requires a higher compression pressure compared to that for gasoline fuel to achieve the threshold condition for autoignition [26,27]. Boronat et al. [28] performed a multidimensional CFD study of the mixing process for LPG fueling. They suggested an improvement in knock resistance via faster combustion due to a higher peak tumble ratio and kinetic energy with a large stroke engine design.

Exhaust gas recirculation (EGR) offers the potential to improve thermal efficiency in SI engines while maintaining the functional compatibility of a three-way catalyst (TWC) after-treatment system. The efficiency benefit of EGR generally results from the reduced heat transfer, low pumping losses, and higher ratio of specific heats (γ) of working fluid [29–31]. However, combustion difficulties are common for about 20% or higher EGR levels in gasoline-fueled SI engines [31,32]. According to Splitter et al. [19], LPG enabled an increased EGR rate compared to gasoline (20-50% relative increase depending on load). The results were attributed to fundamental flame dynamics and combustion properties, such as flame stretch differences between the fuels with EGR. Analysis of CFD simulations by Chuahy et al. [33] showed that propane flames compared to gasoline ones are likely less sensitive to influences from the flow field due to less thickening of the flame and higher effective flame speeds. Various studies [34–36] also investigated the role of EGR as a knock suppression strategy in SI engines as it helps to improve the engine efficiency either by enabling a higher compression ratio or by allowing advanced combustion phasing. Alger et al. [35] demonstrated the advancement of 15 crank angle degrees (CAD) in the combustion phasing with the use of 20% EGR at 8 bar brake mean effective pressure (BMEP). However, Szybist et al. [37] found no combustion phasing advancement benefits with EGR addition at higher loads above 15 bar indicated mean effective pressure (IMEP) for gasoline-fueled operation. The knock suppression benefits of EGR are more visible in low power density (LPD) engines, and there is a substantial kinetic effect of EGR related to the pressure-

101 temperature trajectory of the fuel-air mixture [38]. However, the same magnitude of knock
102 suppression achieved in LPD engines with EGR is not possible in high power density (HPD)
103 engines with gasoline fueling due to potential kinetic limitations of EGR at boosted operating
104 conditions [39,40].
105 To ensure the desired performance of LPG-fueled SI engines with the expected variations in
106 fuel composition, the combustion behavior of the most commonly used LPG blends needs to
107 be characterized. Additionally, utilization of EGR as a knock mitigator for LPG-fueled
108 operation is necessary to investigate considering its kinetic effect related to the in-cylinder
109 thermodynamic states. Therefore, this study first performs an experimental investigation in a
110 spark-ignited cooperative fuel research (CFR) engine with different LPG fuels without and
111 with EGR and evaluates the effects of fuel composition and EGR rate on engine combustion,
112 particularly on end-gas autoignition. For different LPG fuels, mixture autoignition assessment
113 through Livengood-Wu (LW) integral method is then performed to demonstrate the impact of
114 fuel's reactivity on knock occurrence probability. The effectiveness of EGR to mitigate
115 knock with LPG fueling is assessed over the in-cylinder pressure-temperature domain using
116 chemical kinetics modeling. Finally, a numerical three-dimensional (3D) computational fluid
117 dynamics (CFD) model of the test engine is developed for the fundamental understanding of
118 in-cylinder LPG combustion processes with different EGR rates.
119

120 # 2 Experimental Activity

121 ## 2.1 Test set up

122 A single-cylinder, spark-ignited cooperative fuel research (CFR) engine with the variable
123 compression ratio technology was used to conduct experimental investigations. The
124 specifications of the test engine are presented in Table 1. The previous work by the authors
125 [9,41] provides complete details of the test engine setup and its instrumentation and control.

In this work, three different LPG fuels, i.e., Pure propane, EU rep, and US rep, were used for experimental investigations, and their compositions are presented in Table 2. Note that the tested fuels, particularly US rep and EU rep, are chosen because they represent average compositions of different LPG blends used as automotive fuels across the continent [9].

Table 1: Test engine specifications.

Type	CFR F1/F2
No of Cylinder	1
Bore and Stroke	82.55 mm & 114.3 mm
Compression Ratio	Adjustable, 4:1 to 187:1
Number of Valves	2
Valve Overlap	5 crank angle degrees
Mixing System	Air-fuel premixed

Table 2: Composition of the tested LPG fuels.

	Volume (%) of LPG composition		
	Pure Propane	**US rep**	**EU rep**
Methane (CH_4)	-	0.05	-
Ethane (C_2H_6)	-	6.54	-
Propane (C_3H_8)	100	92.65	81.95
Propene (C_3H_6)	-	0.23	-
N-butane (n-C_4H_{10})	-	0.08	18.05
Isobutane (i-C_4H_{10})	-	0.45	-

A cooled, external exhaust gas recirculation (EGR) system was integrated with the test engine to reintroduce the exhaust gas to the intake system [42]. The EGR rate is calculated based on the measured mass flow rates as follow:

$$\text{EGR}\ (\%) = \frac{\dot{m}_{\text{EGR}}}{\dot{m}_{\text{total}}} * 100 \qquad (1)$$

where $\dot{m}_{EGR}$ is the EGR mass flow rate and $\dot{m}_{total}$ is the total mass flow rate combining fresh air, test fuel, and recirculated exhaust gas.

High-speed, crank angle resolved in-cylinder pressure data was acquired using a water-cooled piezoelectric transducer (Kistler 6061B). Intake and exhaust absolute pressures were also measured using two dynamic sensors, Kistler 4007D and 4049B, respectively. A rotary encoder with 0.1 crank angle degrees (CAD) resolution was used to record 1000 full engine cycles. These high number of cycles are required to capture the knocking events with a high level of statistical accuracy. A large engine control module (LECM) from Woodward Inc. and a customized LabView firmware were incorporated to control and monitor engine operation.

2.2 Test methodology

In this study, a premixed air-fuel (gaseous) mixture was supplied to the intake manifold to run the test engine at different compression ratios. For all engine operating conditions, ignition timing was varied to maintain the location of 50% mass fraction burned (i.e., CA50) in between 9 to 10 deg aTDC. An overview of the test plans, including engine operating conditions, is presented in Table 3.

Table 3: Experimental test matrix.

Test type	Fuel	Compression Ratio	IMEP (kPa)	Intake Manifold Pressure (kPa)	Speed (RPM)	λ	EGR rate (%)	Others
Fuel composition effect	Pure Propane, EU rep, US rep	7, 10	Varied	101.2 (fixed)	900	1	–	Intake mixture Temp: 60 ^{0}C Coolant Temp: 95 ^{0}C Oil Temp: 57 ^{0}C
EGR effect	Pure Propane, EU rep	8	1000 (fixed)	Varied			0 - 30	

An in-house built LabView code was used to perform the power spectrum analysis of the bandpass filtered pressure signal based on the FFT technique and to report a summation value of the maximum amplitude of power spectrum for 200 consecutive engine cycles in real-time

159 during engine testing for each operating condition [42,43]. This reported value was called
160 knock integral (KL), which quantifies the knocking intensity. The authors found that the
161 value of KL ~ 5 kPa^2 indicates the borderline or trace knock condition based on the
162 judgement of audible sounds from the CFR engine. A Butterworth type bandpass filter with
163 lower and upper cut-off frequencies equal to 3 and 20 kHz, respectively, was used to capture
164 all significant high-frequency spectral components of the pressure signal [44]. Various other
165 metrics of knocking combustion, such as the maximum amplitude of high-frequency pressure
166 oscillation (MAPO), knock point (KP), and knock point pressure (KPP), were also evaluated.
167 MAPO was calculated based on the maximum absolute amplitude of the bandpass filtered in-
168 cylinder pressure related to knock. KP is the crank angle location where a sharp inflection
169 occurs in the cylinder pressure trace before the onset of high-frequency pressure oscillations.
170 The KP of each engine cycle was estimated as the crank angle corresponding to the peak of
171 the second derivative of in-cylinder pressure [41,45].

172 In this work, a single, representative in-cylinder pressure trace for the *non-knocking condition*
173 was selected from all recorded 1000 cycles by minimizing the $COST_{NK}$ function [46], as
174 defined in Equation 2.

$$\mathrm{COST}_{NK}\ (\mathrm{i}) = \left[\left(\frac{\mathrm{IMEP_i} - \mathrm{IMEP_{avg}}}{\mathrm{IMEP_{avg}}}\right)^2\right] + \left[\left(\frac{\mathrm{PP_i} - \mathrm{PP_{avg}}}{\mathrm{PP_{avg}}}\right)^2\right] \qquad (2)$$

175 where IMEP is the indicated mean effective pressure, PP is the peak in-cylinder pressure, and
176 the subscripts i and avg denote the i^{th} cycle and the average quantity (evaluated from all 1000
177 cycles), respectively.

178 For the *knocking condition*, the top four measured, in-cylinder pressure traces with minimum
179 $COST_K$ were initially identified based on Equation 3. The power spectral density (PSD) of
180 each of the four traces was then compared with the average PSD of all recorded 1000 cycles

[47]. The candidate cycle with PSD similar to the average spectrum was chosen as the final knocking representative pressure trace that is to be used for comparison with CFD results.

$$\mathrm{COST}_K\,(\mathrm{i}) = \frac{\left|\left(dp/dt\right)_{max}^{i} - \left(dp/dt\right)_{max}^{avg}\right|}{\left(dp/dt\right)_{max}^{avg}} + \frac{\left|\mathrm{E}_{res}^{i} - \mathrm{E}_{res}^{avg}\right|}{\mathrm{E}_{res}^{avg}} + \frac{\left|\mathrm{MAPO}_i - \mathrm{MAPO}_{avg}\right|}{\mathrm{MAPO}_{avg}} \quad (3)$$

where $(dP/dt)_{max}$ is the maximum pressure rise rate used to characterize the uniform in-cylinder pressure rise. MAPO is the maximum amplitude of pressure oscillations of the bandpass filtered pressure [48,49], and E_{res} is the energy of resonance associated with a high-frequency pressure signal [50]. Both MAPO and E_{res} describe the unsteady pressure field.

3 Numerical Methodology

3.1 Chemical kinetic model

ANSYS Chemkin-Pro software package [51] was used as a reaction kinetic solver to perform different kinetic evaluations, such as ignition delay and laminar flame speed. A closed, constant volume homogeneous 0-D batch reactor with adiabatic and chemically inert walls was used to calculate ignition delay time (IDT) of the air-fuel mixture representing the in-cylinder trapped charge for the pressure and temperature conditions found in the engine cycles. IDT is defined as the time corresponding to maximum OH species concentration generation in the reactor [23,51]. An adiabatic, freely propagating flame model was used to calculate laminar flame speeds corresponding to different state conditions found in the CFR engine. Note that the in-cylinder pressure measured during engine experiments and the unburned gas temperature determined by the GT-Power three pressure analysis (TPA) model were used as input pressure and temperature in the kinetic model. Measured fuel and exhaust gas composition volumes were also used as simulation inputs. A reduced chemical kinetic mechanism including NO chemistry (consisting of 153 species and 1227 elementary reactions) developed from the detailed NUIGMech1.1 mechanism based on the ignition delay

and laminar flame speed studies by Slunecka et al. [52,53] was used in the chemical kinetic model.

In this study, the Livengood and Wu (LW) method [54–56] was used to study the end-gas autoignition probability of a trapped charge via calculated ignition delay using the in-cylinder pressure-temperature trajectory of a given engine operating condition. The LW integral describes the evolution of a specific mixture towards ignition, considering the information related to the kinetics of oxidation reactions under specific pressure-temperature conditions for a given mixture composition. As postulated by Livengood and Wu [54], the amplitude of the considered ignition carriers would only increase towards its critical value at ignition according to a specific time delay (τ), and LW integral can be expressed as :

$$1 = \int_0^{\tau_{ign}} \frac{1}{\tau}\, dt \qquad (4)$$

where τ_{ign} is the time delay until ignition and τ is the instantaneous ignition delay time. If the LW integral of Equation 4 reaches or comes close to 1, the air-fuel mixture will be subject to autoignition under those conditions of temperature and pressure due to the high concentration of ignition carriers [56].

3.2 CFR engine model

In this study, a 0D/1D simulation model of the CFR test engine was developed based on the three-pressure analysis (TPA) method using Gamma Technologies' GT-Power software platform [41,57,58], as shown in Figure 1. The TPA model, which incorporates the two-zone combustion concept and Woschni's heat transfer correlation, performs the *non-predictive combustion simulations* (based on chemical equilibrium calculation) using the measured, crank angle resolved intake, exhaust, and in-cylinder pressure (cycle-averaged) as well as other experimental data, including exhaust compositions, time-averaged temperatures of intake, exhaust, and cooling systems. The model validation was performed by comparing the

simulated inducted charge mass and in-cylinder pressure with those obtained from experiments. Figure 2 shows a comparison of in-cylinder pressure from experiments and non-predictive simulations for propane fueling without and with EGR at CR 8, and a close agreement between the results confirms the accuracy of the TPA model. The residual gas fraction and wall temperatures obtained from this 0D/1D model were then used as initial and boundary conditions for the subsequent 3D CFD simulations.

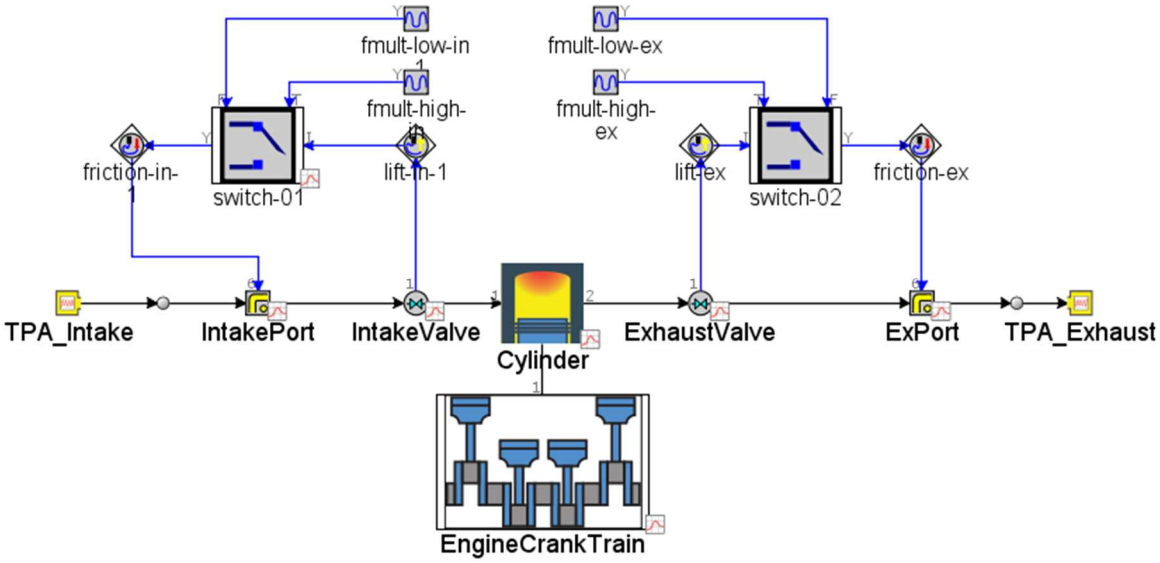

Figure 1: Three pressure analysis (TPA) 0D/1D model of the CFR engine in GT-Power.

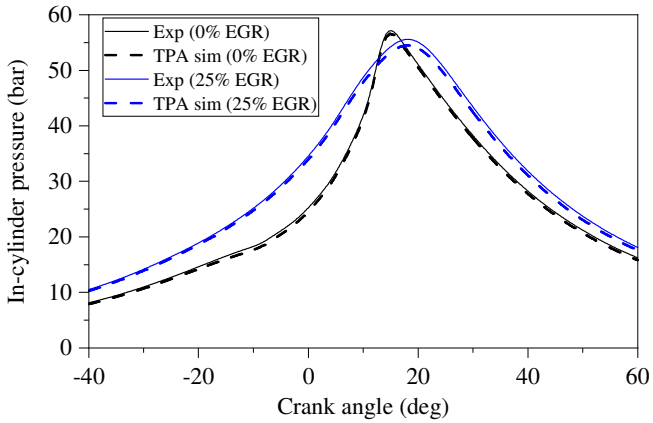

Figure 2: Comparison of cycle averaged in-cylinder pressure with propane fueling without and with EGR at CR 8 obtained from non-predictive TPA simulations and experiments.

A three-dimensional (3D) computational fluid dynamics (CFD) simulation model of the CFR test engine was developed using CONVERGE software platform (version 3.0.18) [41,47,59,60]. For combustion modeling, the SAGE detailed chemistry solver [61] was implemented in the unburned zone to capture end-gas autoignition. The G-equation based chemical equilibrium (CEQ) model was incorporated on flame, and the model tracks the turbulent flame front in a Eulerian manner by solving the transport equation for the Favre-averaged mean of the non-reacting passive scalar *G* [62] based on the flamelet theory of turbulent premixed combustion [63]. The incipient spark kernel was modeled by adding a volumetric source for a passive scalar G. Furthermore, the turbulent flame speed is calculated based on Equation 5 in the RANS context [63].

$$S_t = S_l + u' \left\{ -\frac{a_4 b_3^2}{2b_1} Da + \left[\left(\frac{a_4 b_3^2}{2b_1} Da \right)^2 + a_4 b_3^2 Da \right]^{1/2} \right\} \quad (5)$$

where u′ is the turbulent velocity fluctuation, S_l is the laminar flame speed, Da is the Damköhler number, and a_1 and b_1 are modeling constants. The value of $b_1 = 2.5$ was used in this work for model calibration.

In-cylinder turbulence was modeled using the Reynolds-averaged Navier-Stokes (RANS) based renormalized group (RNG) k-ϵ model [64]. Wall heat transfer was captured using the model proposed by O′Rourke and Amsden [65]. The grid control strategy of the current computational domain was adopted as per our previous work [41]. The model incorporates the 153 species reduced chemical kinetic mechanism, including the NO chemistry for LPG combustion [52]. This reduced mechanism was also used to generate a lookup table of laminar flame speeds as a function of pressure, temperature, and equivalence ratio using the CONVERGE 1D laminar flame speed solver [59]. A comparison of the percentage difference in the calculated laminar flame speed (S_L) by Converge and Chemkin solvers using the reduced chemical mechanism is presented in Figure 3 for pure propane, EU rep, and US rep

261 at the different temperature, pressure, and EGR conditions. As shown, apart from low
262 pressure and high EGR conditions, flame speeds calculated by Converge are within 3% of
263 those obtained from Chemkin, indicating a reliable accuracy of the Converge 1D flame speed
264 calculation solver. Therefore, the laminar flame speed lookup table created by the Converge
265 solver was implemented in the G-equation model.

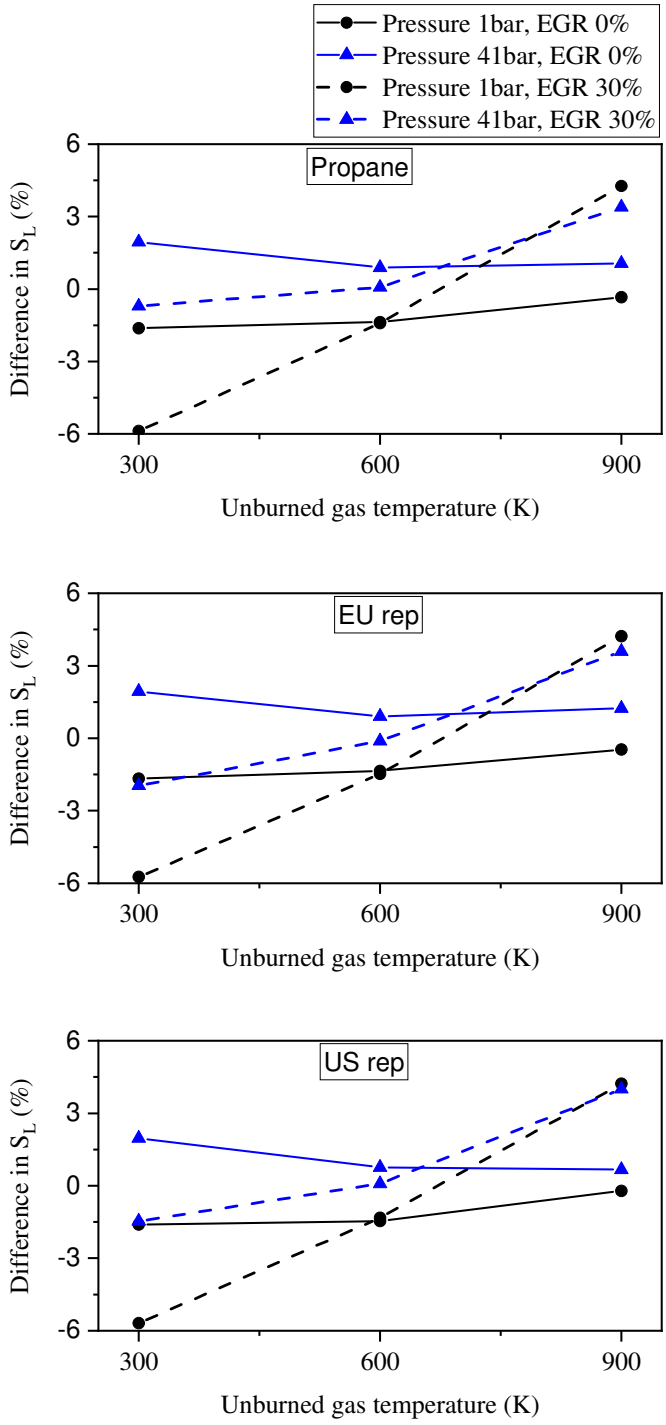

Figure 3: Difference in laminar flame speed (S_L) calculated by Converge and Chemkin solvers for pure propane (top), EU rep (middle), and US rep (bottom) at different operating conditions.

It is now necessary to verify initial CFD model results before performing detailed simulation calculations for different engine operating conditions. A comparison of in-cylinder motoring and firing pressure obtained from experiments and CFD simulations are presented in Figure 4

and Figure 5, respectively. At CR 7 and 10, in-cylinder motoring pressure traces are reasonably predicted by the simulations, which confirms a reasonable accuracy of the compression ratio setup used in the CFR engine model. It is essential as the CFR engine has variable compression ratio technology. Furthermore, as shown in Figure 5, the predicted in-cylinder firing pressure traces are well within the span of measurement limits. This suggests that the 3D CFD model can further be used to simulate LPG combustion processes, particularly end-gas autoignition.

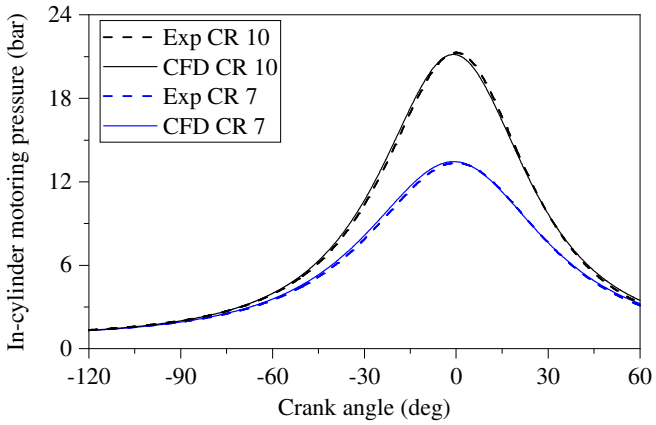

Figure 4: Comparison of in-cylinder pressure (motoring) obtained from experiments and CFD simulations at CR 7 and 10.

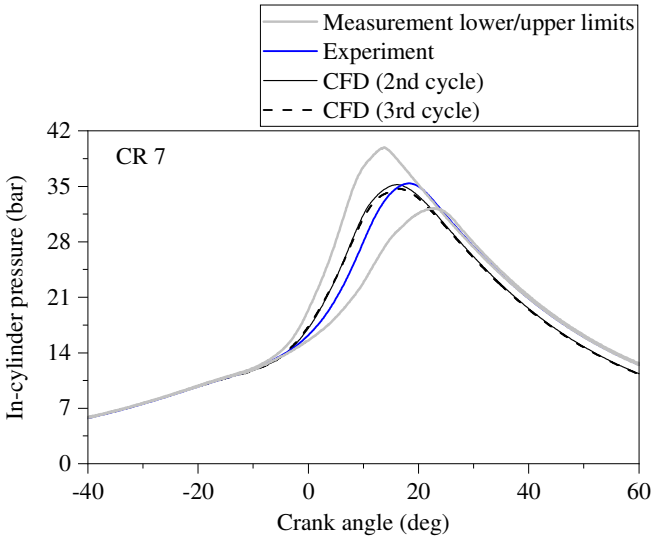

Figure 5: Comparison of in-cylinder pressure (firing) obtained from experiments and CFD simulations for EU rep fueling at CR 7.

4 Results and discussion

4.1 Effect of fuel composition

In this section, the effects of LPG fuel composition on various combustion characteristics are analyzed at CR 7 and 10 for a constant engine speed and intake manifold pressure condition (i.e., 900 RPM and 101.2 kPa).

4.1.1 In-cylinder pressure and knock propensity

Figure 6 presents a comparison of measured, representative in-cylinder pressure traces obtained with pure propane, US rep, and EU rep fueling at CR 7 and 10. As expected, with the increase of compression ratio, in-cylinder pressure increases, and the location of peak pressure moves closer to TDC for all fuels. Unlike CR 7, a sharp inflection point in the slope of pressure trace,

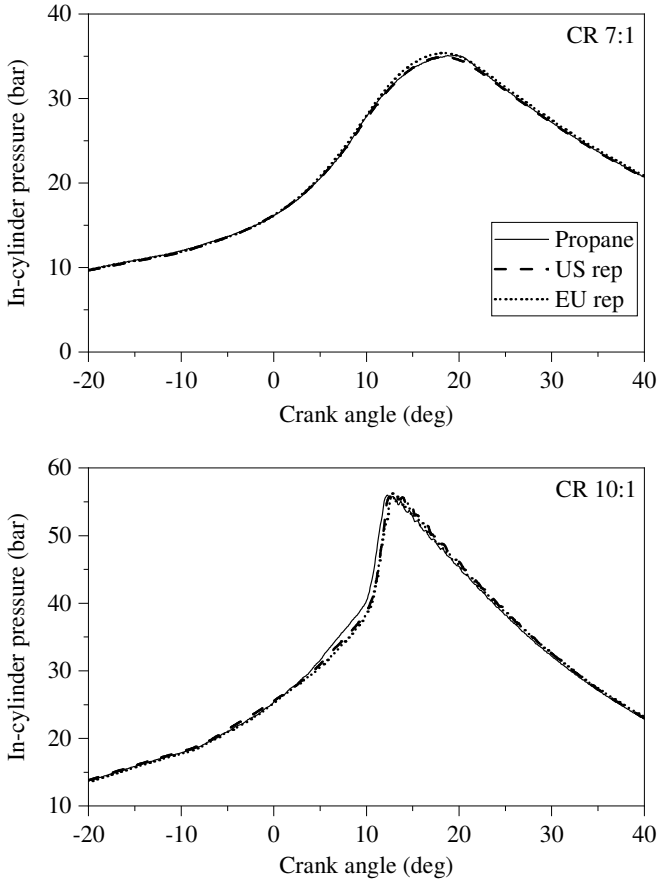

297

298 Figure 6: Comparison of measured, representative in-cylinder pressure with propane, US rep, and EU
299 rep fuelling for CR 7:1 (top) and CR 10:1 (bottom) at 900 RPM, λ=1.

300 i.e., an increase in the rate of pressure rise, is observed for all fuels at CR 10, indicating a
301 likelihood of end-gas autoignition.

302 The variations of knock propensity at different compression ratios for pure propane, US rep,
303 and EU rep are presented in Figure 7. The occurrence and level of knocking are determined
304 using the knock integral (KL) parameter by analyzing the maximum amplitude of power
305 spectrum over the recorded cycles based on the FFT analysis of bandpass filtered pressure
306 trace, as described in Section 2.2. The maximum amplitude of power spectrum variations is
307 minimal at a low compression ratio, i.e., CR 7. All the LPG fuels exhibit KL lower than the
308 borderline knock limit (i.e., $KL_{Knock\ limit} \sim 5\ kPa^2$), indicating a normal combustion state
309 without knocking. At CR 10 (high compression ratio case), the power spectrum amplitude
310 significantly

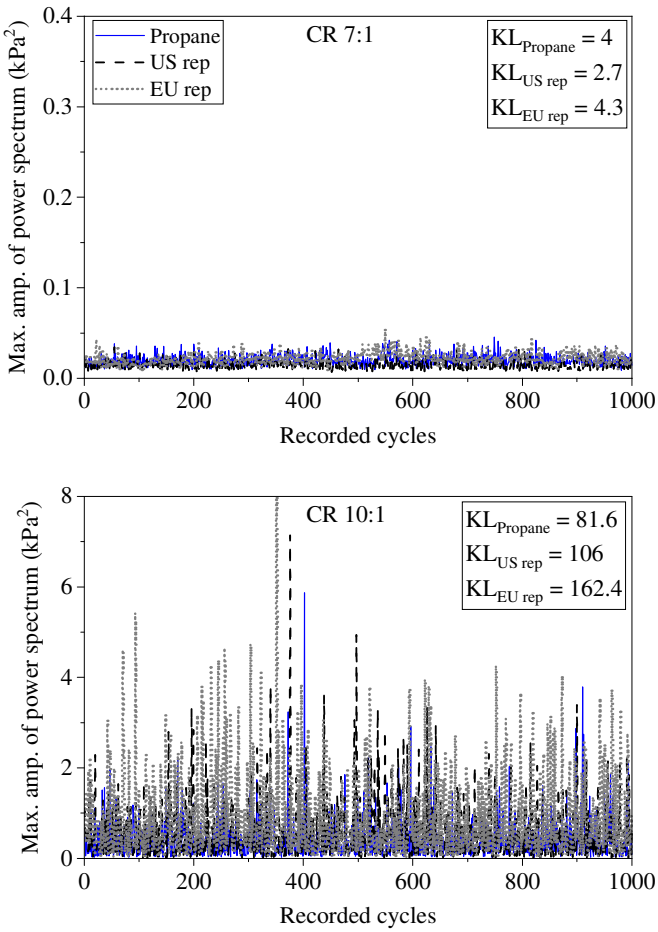

311

312 Figure 7: Maximum amplitude of power spectrum and knock integral (KL) with propane, US rep, EU
313 rep fuelling for CR 7:1 (top) and CR 10:1 (bottom) at 900 RPM, λ=1.

314 increases and KL >> $KL_{Knock\ limit}$ for all tested fuels, implying highly knocking conditions. A
315 higher compression ratio increases the in-cylinder pressure and temperature that may lead to
316 autoignition of the unburned-fuel air mixture and, therefore, knocking combustion. Among
317 the tested fuels, the knock integral follows the trend as $KL_{EU\ rep}$ > $KL_{US\ rep}$ > $KL_{Pure\ propane}$ and
318 EU rep fuel exhibits the highest knock intensity likely due to a high percentage of reactive C4
319 alkane (i.e., n-butane) in the mixture.

320 Additionally, Figure 8 shows the distribution of the maximum amplitude of bandpass filtered
321 high-frequency pressure oscillation (MAPO) for all the tested fuels at CR 10 over the
322 recorded engine cycles. Consistent with KL observations, EU rep demonstrates the largest

variations in high-frequency pressure oscillations due to end-gas autoignition. The average MAPO trend follows as $MAPO_{EU\ rep} > MAPO_{US\ rep} > MAPO_{Pure\ propane}$.

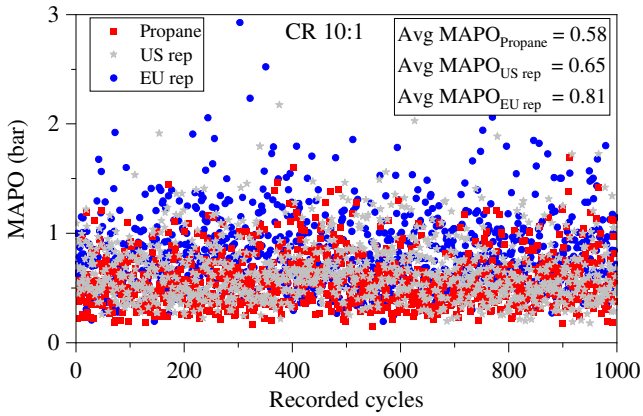

Figure 8: MAPO for pure propane, US rep, and EU rep fuels at CR 10.

The observed knocking behavior is now correlated with the knock resistance property of the tested fuels in terms of methane number, as shown in Figure 9. Methane number (MN) is defined as the percentage by volume of methane blended with hydrogen that exactly matches the knock intensity of the unknown gas mixture under specified operating conditions. The MN of gaseous LPG fuels is calculated using the MWM MN calculation program by EUROMOT [66]. Note that the calculated MN of US rep fuel is similar to that of pure propane despite containing a lower volume percentage of propane (~92.65%), which is likely due to the calculation assumption of iso-butane having the same knock resistance as n-butane with an MN of 10 [8] and the presence of ethane with higher MN. As shown, EU rep fuel has methane no of 30, which is less resistant to end-gas autoignition than pure propane with methane no of 34. This supports the experimental observations of EU rep having the maximum knock tendency ($KL_{EU\ rep}$ ~162.4 kPa^2) and pure propane with minimum propensity ($KL_{Pure\ propane}$ ~ 81.6 kPa^2).

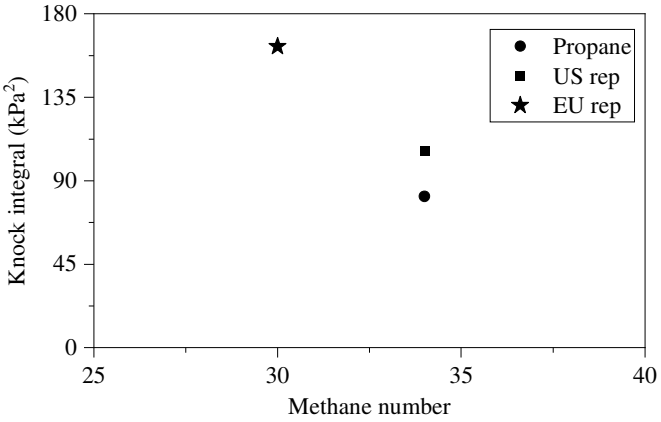

340

341 Figure 9: Knock integral at CR 10 vs. calculated methane number for all the tested fuels.

342

343 **4.1.2 Reactivity of the tested fuels**

344 In this section, the reactivity of the tested fuels is evaluated to understand their impact on
345 combustion processes, particularly on end-gas autoignition. Most of the previous reactivity
346 studies [24,52,67] related to LPG blends are evaluated with conditions different from the
347 actual thermodynamic conditions found in SI engines. Therefore, it is an important
348 consideration to study the fuel reactivity for actual in-cylinder thermodynamic conditions.
349 Figure 10 presents the pressure-temperature (P-T) trajectories based on measured, cycle-
350 averaged in-cylinder pressures and unburned zone gas temperatures estimated by the non-
351 predictive TPA model for all the tested fuels at CR 10. Note that the highlighted RON and
352 MON regimes are for conventional gasoline fuel [38] and represent a wide range of engine
353 operating conditions in the pressure-temperature space. The in-cylinder P-T trajectories of
354 LPG fuels are placed on the 'Beyond MON' region, which indicates higher temperatures than
355 the RON trajectory for the same pressure condition. A portion of the P-T trajectory ranging
356 from the location of spark to the knock point is primarily used for ignition delay time
357 evaluations.

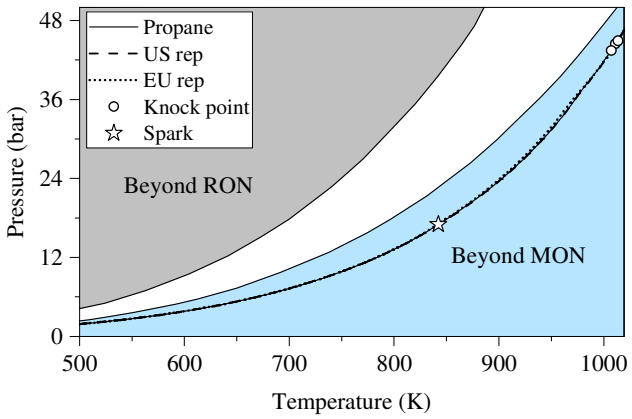

358

359 Figure 10: Pressure - temperature trajectory in the unburned zone for each tested fuel at CR 10:1, 900
360 RPM, and λ=1. Standard RON and MON regions of conventional fuel were taken from [38].

361 Figure 11 presents the results from the constant volume, homogeneous reactor simulations for
362 individual species found in the tested fuels corresponding to the pressure-temperature
363 trajectory of EU rep fuel at CR 10. The results highlight the effect of each species' molecular
364 structure on ignition delay time (IDT) in the engine-relevant high temperature and pressure
365 regime. As expected, methane and ethane have higher IDT, i.e., lower reactivity than propane
366 due to their compact structure. On the other hand, butane's reactivity is more substantial than
367 that of propane at relatively low temperatures, which can be attributed to butane's significant
368 low-temperature oxidation chemistry due to longer carbon-chain length [23,24]. However,
369 the difference in the reactivity between propane and butane is less at high temperatures.
370 Propene also exhibits a significant reactivity at this high-temperature zone due to the
371 presence of a secondary hydrogen atom associated with the weak C-H bond [68]. This
372 understanding of individual species reactivity is necessary to explain the specific trends in the
373 overall reactivity of the tested fuels.

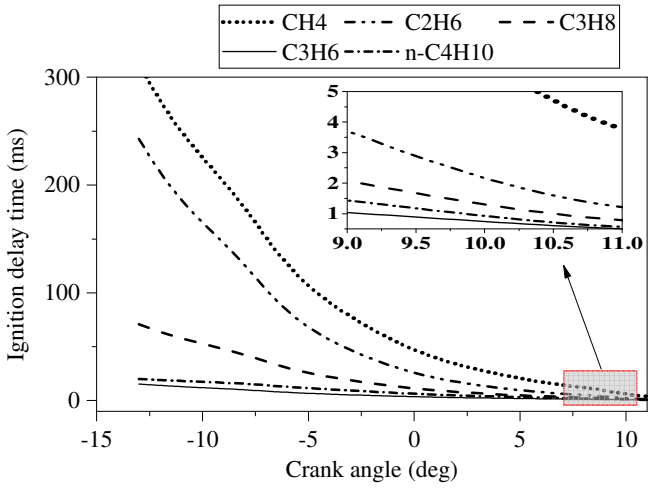

Figure 11: Ignition delay time (IDT) of different species present in the tested fuels corresponding to the pressure-temperature trajectory of EU rep fuel at CR 10.

Figure 12(a) presents the reactivity of the tested fuels in terms of the calculated ignition delay time for the pressure-temperature trajectory of EU rep fuel at CR 10. This single P-T trajectory is initially employed for all fuels to investigate only the effect of fuel composition variation on the fuel reactivity by isolating the in-cylinder thermodynamic condition effects. As shown, EU rep fuel is the most reactive among all the tested fuels due to the presence of a high percentage of reactive C4 alkane (i.e., n-butane) in the mixture. The reactivity of US rep fuel is similar to that of pure propane despite the presence of reactive C4 alkanes and propene in its mixture. This could be attributed to the presence of a significant amount of less reactive ethane (~ 6.54 % by volume) in the US rep blend. However, global fuel characteristics are controlled by the major components in the LPG blends. For example, Morganti et al. [69] observed that the octane number for a specific LPG fuel blend is associated with the main components of the fuel, which is also consistent with the findings of similar methane number (MN) for both Propane and US rep fuel (Figure 9). Furthermore, considering both the effect of fuel composition and in-cylinder thermodynamic conditions of the respective fuel, it has been observed that the reactivity of the tested fuels at CR 10 case follows the trend as EU rep > US rep > Pure propane, as shown in Figure 12(b).

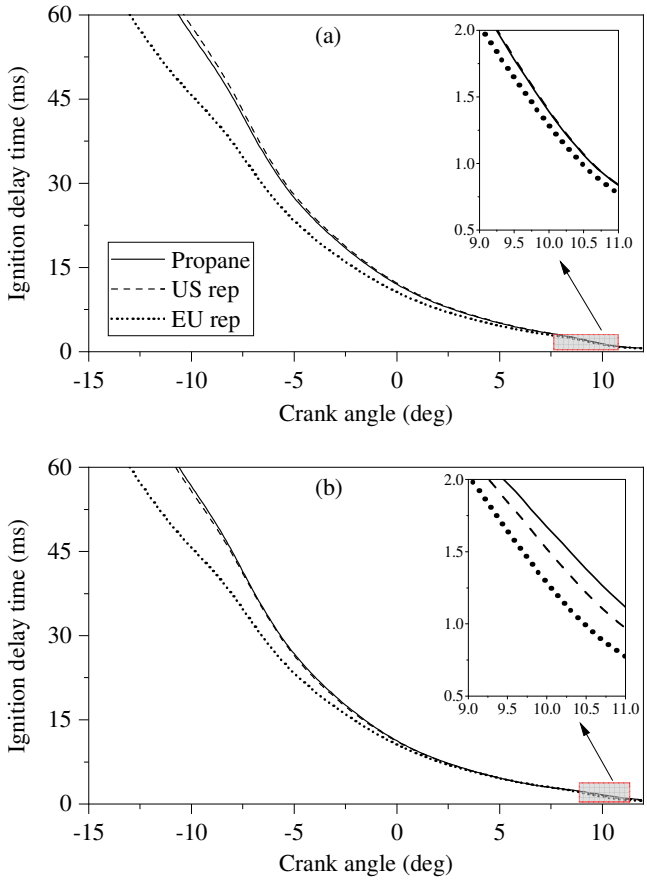

Figure 12: Ignition delay time of the tested fuels for the pressure-temperature trajectory of (a) EU rep fuel and (b) individual fuel at CR 10.

As mentioned in Section 3.1, the Livengood-Wu (LW) integral is a widely accepted approach for evaluating the knock-occurrence probability in the unburned zone of internal combustion engines [55,56]. Figure 13 presents the LW integral for each tested fuel based on the calculated ignition delays, considering their respective pressure-temperature trajectory at two different compression ratios. According to this method, when the value of LW integral equals to one, it marks the start of end-gas autoignition during the SI engine combustion process. At CR 10, the integral value of all the fuels has reached to 1. This indicates that the concentration of ignition carriers in the mixture arrives at their critical values, resulting in obvious end-gas autoignition. On a fuel basis, EU rep being the most reactive fuel reaches early to the critical LW integral value of 1, demonstrating its high propensity towards the

406 end-gas autoignition among the tested fuels. At CR 7 (Figure 13-b), the final values of the
407 LW integral are well below the critical mark of 1, suggesting that the in-cylinder
408 thermodynamic conditions are not conducive enough to initiate any end-gas autoignition
409 process in the unburned zone. This knock occurrence probability prediction for the tested
410 fuels by the LW approach is in accordance with the experimental observations, as shown in
411 Figure 7 for CR 7 and 10. Furthermore, as shown in Figure 14, the predicted knock point
412 (KP) locations by the LW method (i.e., the crank angle corresponding to LW integral equal to
413 one) are within 2 CAD of those calculated from measured, in-cylinder pressure traces using
414 the 2nd order derivative method at CR 10 for all the tested fuels.

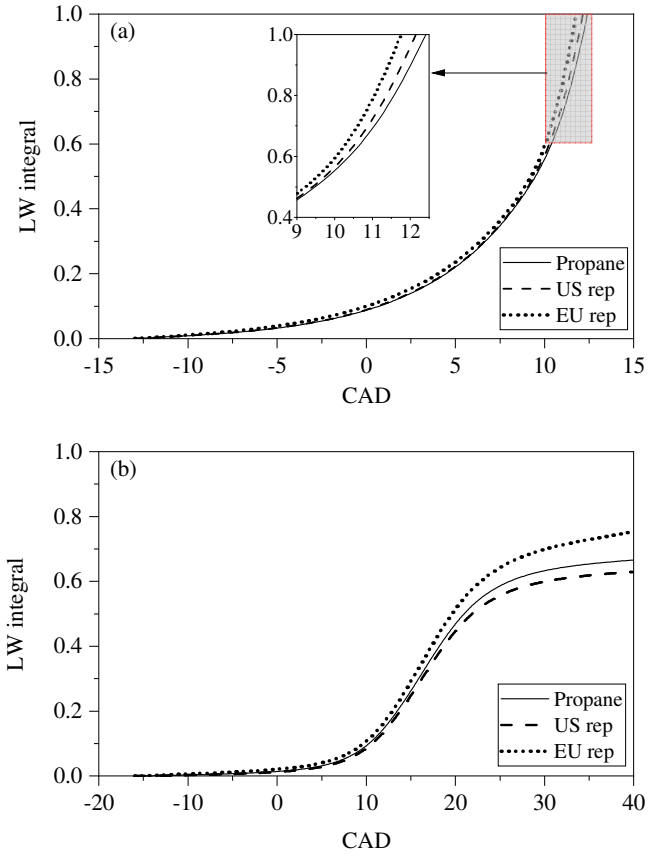

415

416 Figure 13: LW integral for all tested fuels corresponding to their respective pressure-temperature
417 boundary conditions at (a) CR 10 and (b) CR 7.

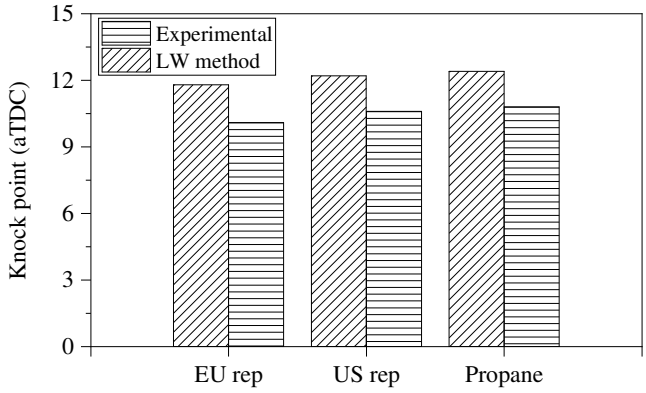

418

419 Figure 14: Comparison of knock point locations predicted by the LW method via ignition delay and

420 the 2nd order derivative method using measured pressure traces at CR 10 for all the tested fuels.

421

422 **4.1.3 CFD model prediction of knock characteristics**

423 In this work, 3D CFD simulations were performed for four consecutive full engine cycles, out

424 of which the first cycle was discarded for the analysis to remove any effect of initial

425 conditions. Figure 15 (a) shows in-cylinder pressure traces for simulated engine cycles along

426 with all the 1000 recorded cycles during experiments at CR10 with EU rep fueling. The

427 representative cycle selected from those recorded cycles based on Eq. 3 for the knocking

428 conditions is also presented. As shown, in-cylinder pressure traces predicted by the

429 simulations are well within the spread of measured pressure traces. Furthermore, the

430 simulated cycles exhibit sudden changes in the slope of the in-cylinder pressure traces before

431 the onset of high-frequency pressure oscillations similar to those observed with experimental

432 cycles. A quantitative comparison of the location of the knock point presented in Figure 15(b)

433 demonstrates that the knock points predicted by the simulations are in good agreement with

434 the experimental results with an error of less than 1 crank angle degree (CAD).

435

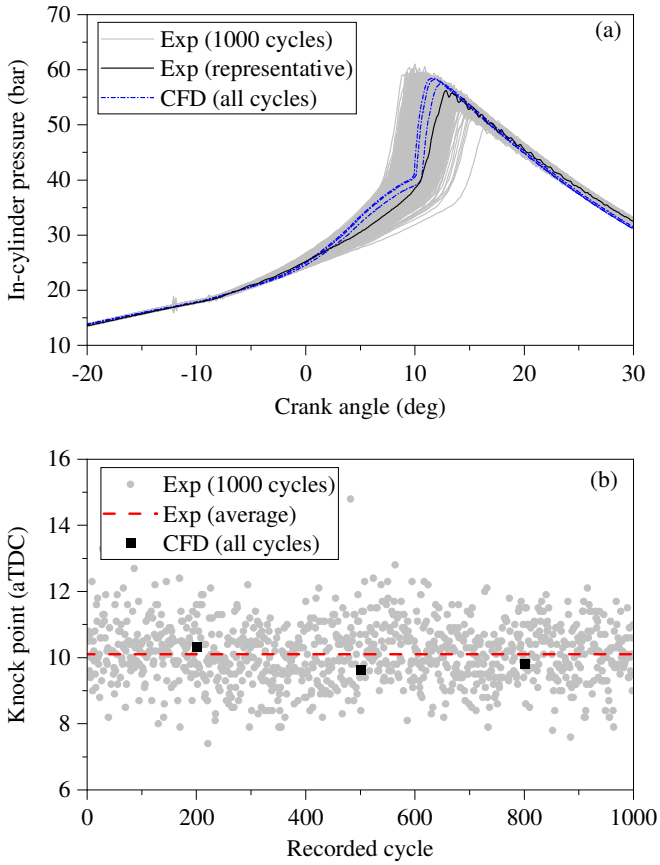

436

437 Figure 15: (a) In-cylinder pressure and (b) knock points from experiments and CFD simulations at CR
438 10 with EU rep fueling. For representation purposes, random cycles are chosen to highlight KP from
439 CFD simulations.

440 Finally, the evolution of in-cylinder intermediate species, radicals, and thermodynamic
441 properties are analyzed for the fundamental understanding of the end-gas autoignition process
442 in detail. It is found in the previous studies [47,70] that formaldehyde (CH_2O) species is a
443 good indicator of intermediate-temperature chemistry, and hydroxyl (OH) radical marks the
444 regions governed by high-temperature chemistry. Figure 16 presents the evolution of in-
445 cylinder temperature and CH_2O and OH species mass fraction on a horizontal cut plane
446 passing through the spark plug for CR 10 case with EU rep fueling over different crank angle
447 instances. These parameters are obtained from the second simulation cycle. At 10.5 deg
448 aTDC, a considerable amount of CH_2O species is built up towards the exhaust valve side,
449 implying an enhanced reactivity of the end-gas. In quick succession, CH_2O is rapidly

consumed and a significant amount of OH species is formed in the end-gas, indicating the start of high-temperature chemistry domination as evidenced by the in-cylinder temperature rise ahead of the propagating flame front due to autoignition. This results in knocking combustion events and subsequent pressure fluctuations, as shown in Figure 6 for CR 10. The results of CH_2O consumption and OH formation when end-gas autoignition occurs are consistent with the observations by [23] for LPG fuels.

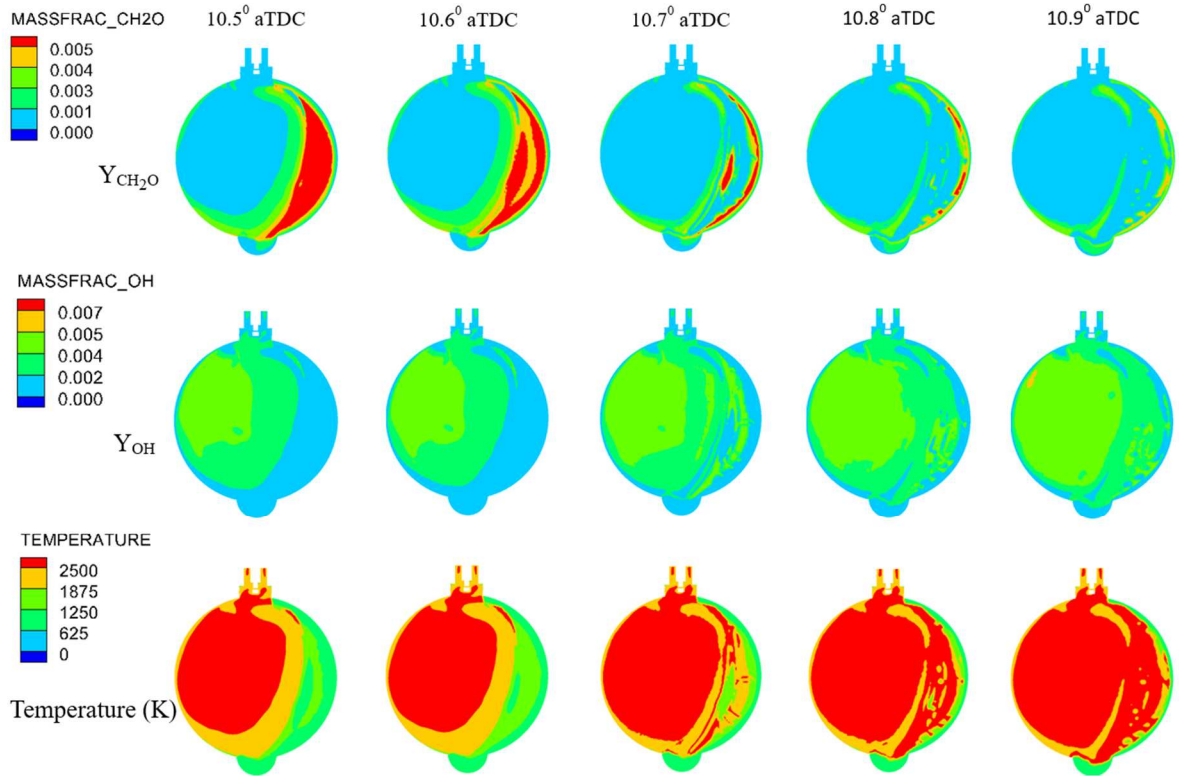

Figure 16: Evolution of CH_2O and OH mass fraction and in-cylinder temperature on a horizontal cut plane passing through the spark plug (obtained from the second simulation cycle). Intake and exhaust are located on the left and right sides, respectively.

4.2 Effect of external exhaust gas recirculation

In this section, the effects of external exhaust gas recirculation (EGR) rate on various combustion characteristics are analyzed for pure propane and EU rep fueling for a constant engine speed and load condition (i.e., 900 RPM and 10 bar IMEP) at CR 8.

4.2.1 In-cylinder pressure and heat release rate

Figure 17(a) presents measured, representative in-cylinder pressure traces for both fuels at CR 8 with 0% and 25% EGR rates. Note that the 25% EGR rate was chosen here as it produced the optimal engine efficiency among the tested EGR rates, and the maximum of 30% EGR rate operation was achieved for both fuels within the accepted combustion stability limit. At the 0% EGR rate, EU rep fuel exhibits the maximum peak in-cylinder pressure, and the sharp inflection points in the slope of pressure traces are observed for both fuels, indicating a likelihood of end-gas autoignition. With EGR, the peak in-cylinder pressure decreases, and the corresponding crank angle location is retarded for both fuels. This is likely due to the prolonged combustion duration as the introduction of EGR decreases the in-cylinder oxygen concentration and, therefore, chemical reaction rate [71]. Note that the required ignition timings are observed in a very similar range for both fuels.

Figure 17(b) presents the apparent heat release rate (AHRR) for propane and EU rep fueling without and with EGR at CR 8. The AHRR is calculated based on the first law of thermodynamics and does not include the heat losses to walls and crevices [20]. As shown, a sharp rise in HRR is observed for both fuels at 0% EGR, with EU rep fuel demonstrating the maximum heat release. Rapid release of energy contained in the end gas due to autoignition ahead of the propagating turbulent flame is likely contributing to the rise in heat release rate. With the increase of EGR rate, the sharp rise in HRR corresponding to the end-gas autoignition diminishes and the overall peak heat release rate also drops for both fuels. As the EGR rate increased, the combustion rate decreased due to lower in-cylinder temperature and reduced oxygen concentration, resulting in a lower heat release rate [6,71]. At the 25% EGR rate, both fuels demonstrate a similar heat release rate despite EU rep being the most reactive among the tested fuels, as found in Figure 12(a).

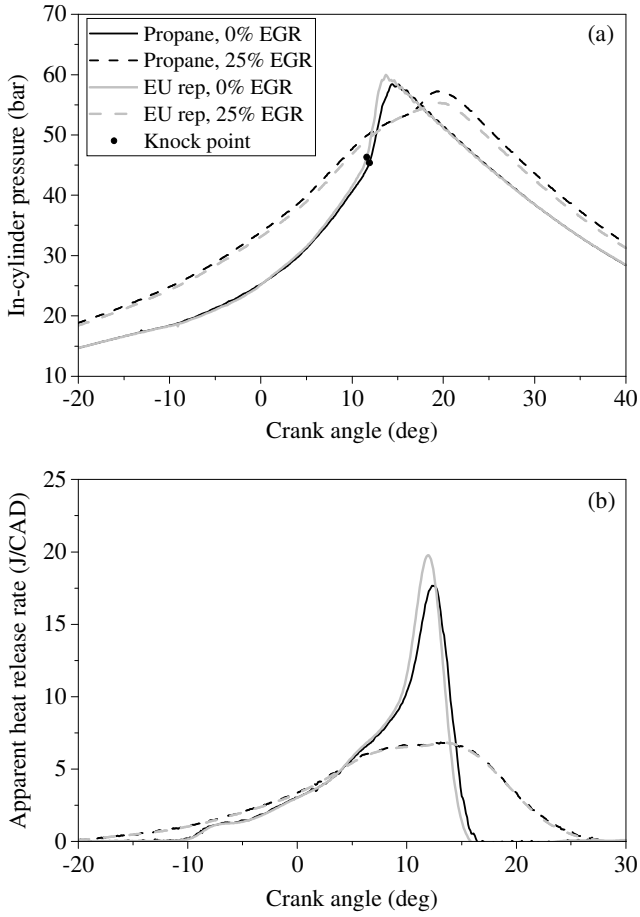

Figure 17: Effect of fuel composition with different EGR rates on (a) representative in-cylinder pressure and (b) averaged apparent heat release rate at CR 8:1, 900 RPM, 10 bar IMEP, and λ=1.

4.2.2 Knock propensity

The influence of EGR rate on the occurrence and intensity of knocking is analyzed by studying the knock integral (KL) and maximum amplitude of pressure oscillations (MAPO), as shown in Figure 18. Both fuels demonstrate higher KL than the $KL_{Knock\ limit}$ (~5 kPa^2) for borderline knock criterion at the 0% EGR rate, confirming knocking conditions. Also, the knock integral of EU rep (i.e., $KL_{EU\ rep}$ ~ 54.3 kPa^2) is higher than that with pure propane (i.e., $KL_{Propane}$ ~ 30 kPa^2), which indicates a higher knock propensity of EU rep fuel and is consistent with the previous observations. This knocking tendency can be reduced using the appropriate EGR rate. As shown, KL for both fuels are similar and below the borderline

502 $KL_{Knock\ limit}$ at 25% EGR rate, indicating normal combustion operation. Additionally, Figure
503 18 (b) shows the maximum amplitude of bandpass filtered high-frequency pressure
504 oscillation (MAPO) for pure propane and EU rep. With the 25% EGR rate, MAPO drops
505 significantly over the recorded cycles for both fuels than those without EGR, with a more
506 substantial impact with EU rep fueling. This can be attributed to lower combustion and end-
507 gas temperatures resulting from the slower chemical heat release and flame propagation of
508 the charged mixture with EGR [72,73]. Therefore, the results demonstrate the potential of
509 EGR as an important knock suppression technology for LPG SI engines.

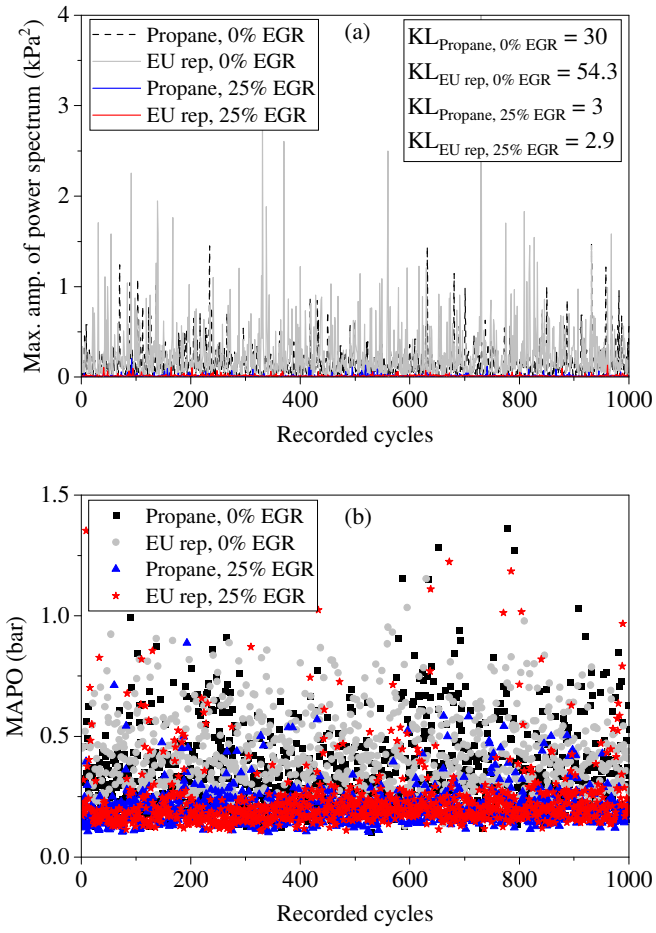

510

511 Figure 18: Effect of fuel composition with different EGR rates on (a) knock integral (KL) and (b)
512 maximum amplitude of pressure oscillations (MAPO) at CR 8:1, 900 RPM, 10 bar IMEP, and λ=1.

513 **4.2.3 Knock mitigation effectiveness of EGR over the pressure-temperature domain**

514 It is now important to understand how the knock mitigation effectiveness of EGR is related to
515 the in-cylinder thermodynamic states and chemical kinetics of fuel. Figure 19 shows the
516 pressure-unburned gas temperature (P-T) trajectories of the propane-air stoichiometric
517 mixture without and with EGR at CR 8. With the 0% EGR rate, the P-T trajectory is in the
518 MON region. With the increase of EGR rate (i.e., 25% EGR), the P-T trajectory moves
519 towards the RON regime as the intake manifold pressure is increased to maintain a constant
520 engine load similar to those with baseline without EGR operation for a given inlet mixture
521 temperature. Additionally, an increase in the ratio of specific heats (γ) of the mixture due to
522 higher EGR rate results in a rise in temperature during the compression stroke, as shown in
523 Figure 20. The combined effect of higher manifold pressure and increased γ with EGR raises
524 the in-cylinder pressure and temperature during the compression stroke. Despite this
525 conducive environment, the 25% EGR rate case is able to suppress the end-gas autoignition
526 (Figure 18), which is likely due to a counter effect of slower kinetic rates with EGR [39,74].
527 Therefore, a further understanding of LPG fuel chemical kinetic interactions with engine
528 operation is necessary.

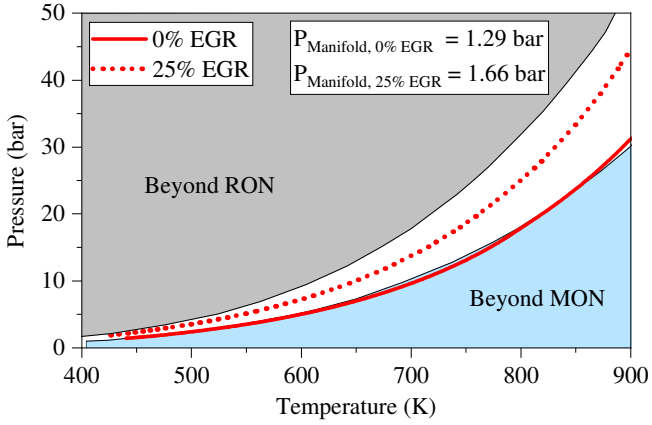

529

530 Figure 19: Pressure-temperature (P-T) trajectories for the stoichiometric propane-air mixture without
531 and with EGR at CR 8. Highlighted regimes correspond to standard RON and MON trajectories of
532 conventional fuel [38].

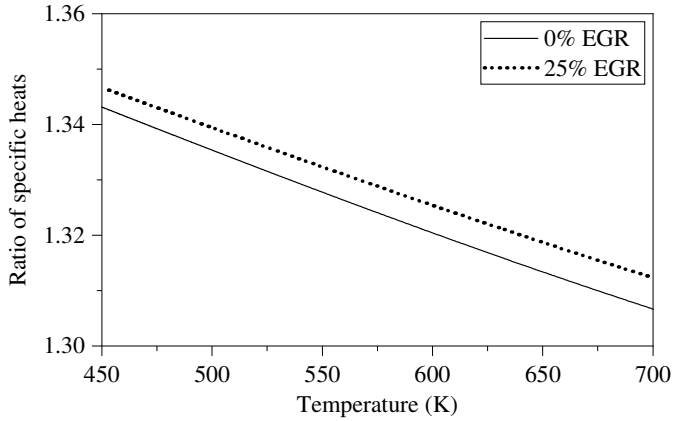

533

534 Figure 20: Ratio of specific heats (γ) of the stoichiometric propane-air mixture (obtained from GT-
535 Power simulations).

536 Figure 21 presents the reactivity of propane without and with EGR in terms of the calculated
537 ignition delay time for the pressure-temperature trajectory at CR 8. The knock onset is related
538 to the ignition delay time of the end-gas [6]. As shown, ignition delay times increase with the
539 increase of EGR rate compared to those with no EGR case, resulting in delayed or suppressed
540 end-gas autoignition reaction (Figure 18). The introduction of EGR causes a decrease in the
541 reactivity of the mixture due to the drop in oxygen concentration and the increase in the heat-
542 sink effect via higher λ, which slows down the chemical reaction rate and, therefore, longer
543 ignition delay time [75].

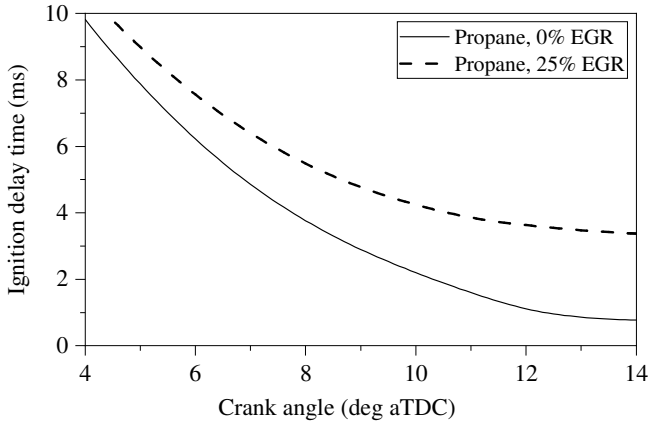

544

545 Figure 21: Ignition delay time for the pressure-temperature trajectory of stoichiometric pure propane
546 combustion without and with EGR at CR 8.

Finally, the knock mitigation effectiveness of EGR for LPG fueling is evaluated using RON and MON regimes over different pressure-temperature trajectories. This is useful to design the EGR strategy for LPG fueling over the operating map as those regimes represent engine operating conditions spanning from naturally aspirated or lightly boosted engines (i.e., 'Beyond MON' space with high temperature and low pressure) to highly boosted, power-dense engines (i.e., 'Beyond RON' space with high pressure and low temperature) [38,76].

For a general understanding of fuel chemical kinetics interaction with engine operation, an example of ignition delay time (IDT) profile of conventional SI engine fuel is presented in Figure 22, highlighting the possible ignition zones over the pressure-temperature domain. Zone 1 represents the high pressure and low-temperature region, and the nearly vertical ignition delay contours signify its high dependency on temperature. In Zone 2, the ignition delay contours become almost horizontal, indicating the region's high sensitivity to pressure compared to temperature. Zone 3 is characterized by a sensitivity to both temperature and pressure.

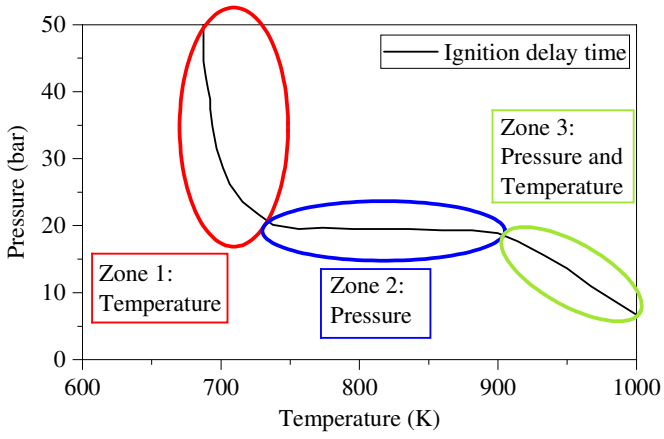

Figure 22: A general example of ignition delay time profile in the pressure-temperature space highlighting the different ignition zones. IDT data was taken from Szybist et al. [38].

In the present study, these zonal-based kinetic interactions on end-gas autoignition are examined for propane combustion without and with EGR using RON and MON regimes, as shown in Figure 23. Here, IDT contours are initially calculated over temperatures ranging

from 600 to 1000 K and pressures of 1 to 50 bar for stoichiometric propane-air mixtures, and an arbitrarily chosen IDT contour corresponding to 10 ms is overlaid on the P-T domain for analysis. Note that a similar study is also possible with a different constant IDT contour. The actual IDT leading to end-gas autoignition is likely to be much shorter as the pressure and temperature of the unburned gas continue to increase. The experimental P-T trajectories for 0% and 25% EGR from Figure 19 are also presented here, where the pressure and unburned gas temperature of both conditions are taken up to the crank angle location of knock point corresponding to the 0% EGR case.

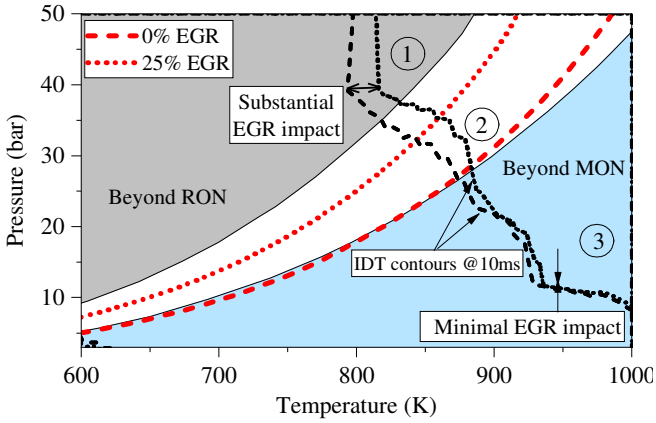

Figure 23: Experimental pressure-temperature trajectories for 0 and 20% EGR for pure propane fuel overlaid on 10 ms ignition delay contours.

As shown in Figure 23, the temperature-sensitive Zone 1 is in the 'Beyond RON' regime of the P-T domain. In this zone, the 10 ms IDT contour needs around 20K higher unburned gas temperature when 25% EGR is added compared to the baseline no EGR condition, indicating an expected knock mitigation effect with EGR in this high pressure and low temperature region (e.g., boosted high load conditions). Next, the pressure-sensitive Zone 2 resides in between RON and MON trajectories. Here, the 25% EGR case exhibits at least a 5 bar higher pressure requirement for end-gas auto ignition to happen corresponding to the 10 ms IDT contour. Thus, EGR is also expected to suppress the knock under these conditions in Zone 2. Finally, the low pressure and high temperature region represented by Zone 3 is in the

587 'Beyond MON' regime of the P-T domain. Unlike Zone 1 and Zone 2, the knock mitigation
588 benefit of EGR diminishes in Zone 3 as can be seen there is no distinct difference in the 10
589 ms IDT contour for both 0% and 25% EGR cases in this low pressure and high temperature
590 region (e.g., light load conditions). Therefore, this zonal-based ignition delay analysis over
591 the P-T domain suggests that EGR is expected to effectively mitigate the end-gas autoignition
592 for operating conditions spanning from the naturally-aspirated engine to highly-boosted,
593 power-dense engine with LPG fueling. Note that this study presents only a specific speed and
594 load condition to assess EGR's knock mitigation utility over the P-T domain, but it is an
595 important first step for LPG fueled engine design with EGR. Further studies over the
596 complete operating map of the engine are required for the final assessment of EGR's knock
597 suppression utility with LPG fueling in the P-T domain.

598 **4.2.4 CFD model prediction with EGR**

599 Figure 24 (a) and (b) present the local evolution of in-cylinder temperature and chemical
600 species (i.e., CH_2O and OH), respectively, for propane fueling without and with EGR at CR
601 8. These CFD results are obtained from the pressure transducer location in the model for the
602 second simulation cycle. At the 0% EGR rate, a sudden consumption of CH_2O and an
603 immediate formation of significant OH species along with the temperature rise in the end-gas
604 indicates the autoignition event for propane fueling, similar to the results shown in Figure 16.
605 However, at the 25% EGR rate, CH_2O consumption is gradual and there is no substantial OH
606 formation in the end-gas. Also, the predicted peak in-cylinder temperature is lower with EGR
607 than that with no EGR condition. These simulation results suggest that the introduction of
608 EGR attenuates the activity related to the onset of end-gas autoignition, which is consistent
609 with the EGR experimental results shown in Figure 18. All of these simulation results (shown
610 in Figure 15, Figure 16, and Figure 24) confirm that the current CFR engine CFD model is

capable to predict both non-knocking and knocking combustion characteristics reasonably well for LPG fuels without and with EGR.

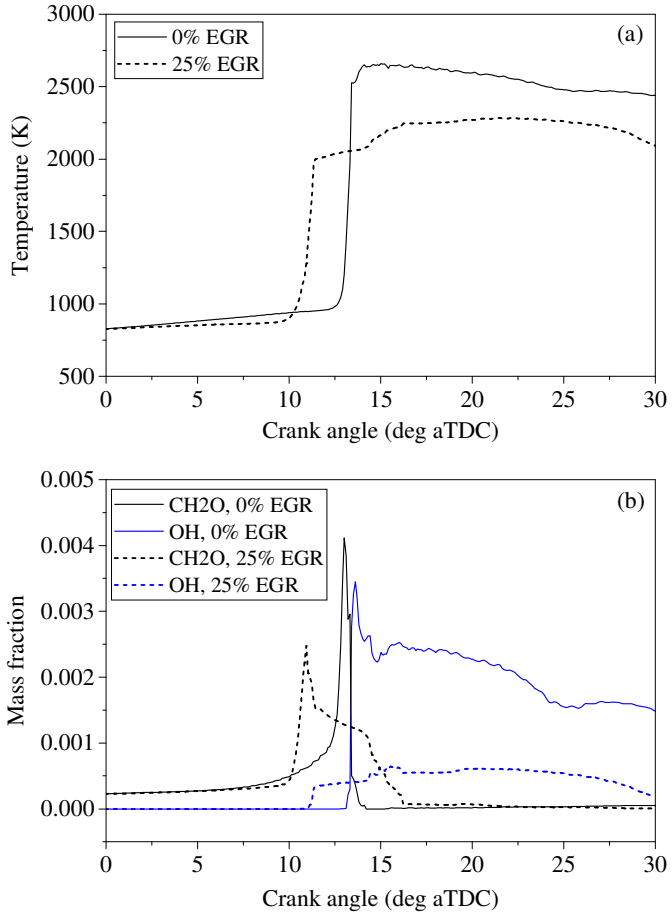

Figure 24: Local evolution of (a) in-cylinder temperature and (b) CH_2O and OH species for propane fueling without and with EGR at CR 8. CFD results corresponds to the pressure transducer location for the second simulated cycle.

5 Conclusion

This paper presented both the experimental and numerical study of a spark-ignited CFR engine fueled with different LPG blends and EGR rates. The effect of LPG fuel composition and EGR rate on combustion characteristics, particularly on end-gas autoignition, were examined for different engine operating conditions. The main conclusions can be summarized as follows.

1. The effect of LPG fuel composition on engine combustion characteristics are initially evaluated at two different compression ratios. Unlike CR 7, a sharp inflection point in the slope of the pressure traces was observed for all fuels at CR 10.
2. Based on the knock integral and MAPO analysis of the tested fuels, CR 7 indicated a normal combustion case, while heavy knocking was observed at CR 10 with EU rep exhibiting the maximum autoignition intensity. This trend was consistent with the knock resistance of fuels in terms of the calculated methane number.
3. Chemical kinetics study considering the effects of fuel composition and in-cylinder thermodynamic conditions demonstrated the reactivity trend of the tested fuels as EU rep > US rep > Pure propane. Based on these, Livengood-Wu (LW) integral method predicted the risk of knock occurrence of individual LPG fuels, which was in line with the experimental observations.
4. With the introduction of EGR at constant IMEP condition, the sharp rise in pressure and heat release rate corresponding to no EGR cases diminishes, and the overall peak of those characteristics drops for both fuels. Also, both KL and MAPO fall below the borderline knock limit for the tested fuels with EGR, with a more substantial impact with EU rep fueling.
5. The knock mitigation effectiveness of EGR was evaluated using the zonal-based kinetic interactions study, which indicated that EGR is expected to effectively mitigate the end-gas autoignition for LPG fueling over the pressure-temperature domain relevant to the current SI engine operation.
6. Finally, the multidimensional CFR engine CFD model was shown to predict the combustion characteristics and demonstrated the evolution of in-cylinder temperature and chemical species. During autoignition of the end-gas, a sudden consumption of CH_2O and an immediate formation of significant OH species along with the

temperature rise were observed for LPG fuel. EGR simulation results showed a substantial drop in such activity, supporting the knock attenuating potential of EGR observed during experiments.

Acknowledgements

This research was funded by the Department of Energy (DOE) and Office of Energy Efficiency and Renewable Energy (EERE) under Award No. DE-EE0009198. The authors would like to thank Colorado State University and the University of Colorado Boulder for providing computing resources in the HPC Summit server. Convergent Science provided CONVERGE licenses and technical support for this work. Cummins Inc. and Argonne National Laboratory are also acknowledged as project partners.

References

[1] Bae C, Kim J. Alternative fuels for internal combustion engines. Proceedings of the Combustion Institute 2017;36:3389–413. https://doi.org/10.1016/j.proci.2016.09.009.

[2] Harry L. Direct Injection of CNG for Driving Performance with Low CO2. 23rd Aachen Colloquium Automobile and Engine Technology, 2014.

[3] Rengarajan S, Liu Z, Lerin C, Stetter J, Narang V, Lana C. LPG Direct Injection Engine for Medium Duty Trucks. SAE Technical Papers 2019:1–10. https://doi.org/10.4271/2020-01-5008.

[4] Matthias NS, Wallner T, Scarcelli R. A Hydrogen Direct Injection Engine Concept that Exceeds U.S. DOE Light-Duty Efficiency Targets. SAE International Journal of Engines 2012;5:838–49. https://doi.org/10.4271/2012-01-0653.

[5] Zhen X, Wang Y. An overview of methanol as an internal combustion engine fuel. Renewable and Sustainable Energy Reviews 2015;52:477–93. https://doi.org/10.1016/j.rser.2015.07.083.

[6] Li X, Zhen X, Wang Y, Liu D, Tian Z. The knock study of high compression ratio SI engine fueled with methanol in combination with different EGR rates. Fuel 2019;257:116098. https://doi.org/10.1016/j.fuel.2019.116098.

[7] Energy Insights n.d. https://www.mckinseyenergyinsights.com/resources/refinery-reference-desk/lpg/.

[8] Krieck M, Günther M, Pischinger S, Kramer U, Thewes M. Effects of LPG Fuel Formulations on Knock and Pre-Ignition Behavior of a DI SI Engine. SAE International Journal of Engines 2015;9:237–51. https://doi.org/10.4271/2015-01-1947.

[9] Fosudo T, Kar T, Marchese A, Windom B, Olsen D. Impact of LPG Composition on Performance, Emissions and Combustion Characteristics of a Spark-ignited CFR Engine. SAE Technical Paper 2022.

[10] Campbell M, Wyszyński ŁP, Stone R. Combustion of LPG in a Spark-Ignition Engine. Source: SAE Transactions, vol. 113, 2004, p. 628–37.

[11] Gomez JE, Walker B, Kerr G. National propane survey final report. 2019.

[12] Yusaf, T., Hussein, I., Zamri, M.Y. and Kuzi A. Experimental work on the use of liquefied petroleum gas in single cylinder petrol engine. SAE Technical Paper 2005.

[13] Murillo S, Míguez JL, Porteiro J, González LML, Granada E, Morán JC. LPG: Pollutant emission and performance enhancement for spark-ignition four strokes outboard engines. Applied Thermal Engineering 2005;25:1882–93.

[14] Lawankar SM. Influence of compression ratio and ignition timing on the performance of LPG fuelled SI engine. SAE Technical Papers 2013;12. https://doi.org/10.4271/2013-01-2889.

[15] Ravi K, Pradeep Bhasker J, Alexander J, Porpatham E. CFD study and experimental investigation of piston geometry induced in-cylinder charge motion on LPG fuelled lean burn spark ignition engine. Fuel 2018;213:1–11.

[16] Chiriac R, Radu R, Niculescu D, Apostolescu N. Development of a LPG fueled engine for heavy duty vehicles. SAE Technical Papers 2003. https://doi.org/10.4271/2003-01-3261.

[17] Campbell M, Wyszyński ŁP, Stone R. Combustion of LPG in a spark-ignition engine. SAE Technical Papers 2004;113:628–37. https://doi.org/10.4271/2004-01-0974.

[18] Karim GA, Wierzba I. Comparative studies of methane and propane as fuels for spark ignition and compression ignition engines. SAE Technical Papers 1983;92:676–88. https://doi.org/10.4271/831196.

[19] Splitter D, Boronat V, Chuahy FDF, Storey J. Performance of direct injected propane and gasoline in a high stroke-to-bore ratio SI engine: Pathways to diesel efficiency parity with ultra low soot. International Journal of Engine Research 2021:1–17.

[20] Heywood J. Internal Combustion Engine Fundamentals. 1988.

[21] ASTM International. Standard Test Method for Research Octane Number of Spark-Ignition Engine Fuel, D2699. 2013.

[22] ASTM International. Standard Test Method for Motor Octane Number of Spark-Ignition Engine Fuel, D2700. 2014.

[23] Smith JR, Green RM, Westbrook CK, Pitz WJ. An experimental and modeling study of engine knock. Symposium (International) on Combustion 1985;20:91–100. https://doi.org/10.1016/S0082-0784(85)80492-6.

[24] Ramalingam AK, Krieck M, Pischinger S, Heufer KA. Understanding the Oxidation Behavior of Automotive Liquefied Petroleum Gas Fuels: Experimental and Kinetic Analyses. Energy and Fuels 2020;34:2323–33.

[25] Badr O, Alsayed N, Manaf M. A parametric study on the lean misfiring and knocking limits of gas-fueled spark ignition engines. Applied Thermal Engineering 1998;18:579–94. https://doi.org/10.1016/S1359-4311(97)00029-X.

[26] Kalghatgi GT, Snowdon P, McDonald CR. Studies of knock in a spark ignition engine with “cars” temperature measurements and using different fuels. SAE Technical Papers 1995;104:1253–67. https://doi.org/10.4271/950690.

[27] Brecq G, Ramesh A, Tazerout M, Le Corre O. An Experimental Study of Knock in a Spark Ignition Engine Fueled with LPG. SAE Technical Papers 2001.

[28] Boronat V, Splitter D, Dal Forno Chuahy F. Achieving Diesel-Like Efficiency in a High Stroke-to-Bore Ratio DISI Engine under Stoichiometric Operation. SAE Technical Papers 2020;2020-April:1–14. https://doi.org/10.4271/2020-01-0293.

[29] Metghalchi M, Keck JC. Burning Velocities of Mixtures of Air with Methanol , Isooctane , and Indolene at High Pressure and Temperature 1982;210:191–210.

[30] Kar, T., Zhou, Z., Brear, M., Yang Y et al. A Comparative Study of Directly Injected, Spark Ignition Engine Combustion and Energy Transfer with Natural Gas, Gasoline, and Charge Dilution. SAE Int J Fuels Lubr 2022. https://doi.org/10.4271/04-15-02-0009.

[31] Caton JA. A comparison of lean operation and exhaust gas recirculation: Thermodynamic reasons for the increases of efficiency. SAE Technical Papers 2013;2. https://doi.org/10.4271/2013-01-0266.

[32] Heywood J. Internal Combustion Engine Fundamentals. 1988.

[33] Dal Forno Chuahy F, Splitter D, Wissink M, Boronat Colomer V. EGR Dilution and Fuel Property Effects on High-Efficiency Spark-Ignition Flames. SAE Technical Papers 2021. https://doi.org/10.4271/2021-01-0483.

[34] Diana, S., Giglio, V., Iorio, B., and Police G. Evaluation of the Effect of EGR on Engine Knock. SAE Technical Paper 1998. https://doi.org/10.4271/982479.

[35] Alger T, Mangold B, Roberts C, Gingrich J. The Interaction of Fuel Anti-Knock Index and Cooled EGR on Engine Performance and Efficiency. SAE International Journal of Engines 2012;5:1229–41. https://doi.org/10.4271/2012-01-1149.

[36] Grandin, B. and Ångström H. Replacing Fuel Enrichment in a Turbo Charged SI Engine: Lean Burn or Cooled EGR. SAE Technical Paper 1999. https://doi.org/10.4271/1999-01-3505.

[37] Splitter D a, Szybist JP. Experimental Investigation of Spark-Ignited Combustion with. Energy & Fuels 2014;28:1432–45.

[38] Szybist JP, Wagnon SW, Splitter D, Pitz WJ, Mehl M. The Reduced Effectiveness of EGR to Mitigate Knock at High Loads in Boosted SI Engines. SAE International Journal of Engines 2017;10. https://doi.org/10.4271/2017-24-0061.

[39] Szybist J. Knock Mitigation Effectiveness of EGR across the Pressure-Temperature Domain. SAE Technical Papers 2020. https://doi.org/10.4271/2020-01-2053.

[40] Kalghatgi GT. Fuel Anti-Knock Quality - Part I. Engine Studies. SAE Technical Paper 2001.

[41] Kar T, Fosudo T, Slunecka C, Marchese A, Windom B, Olsen D. A Study of Propane Combustion in a Spark-ignited Cooperative Fuel Research (CFR) Engine. SAE Technical Paper 2022.

[42] Bayliff SM. Evaluation of controlled end-gas autoignition with exhaust gas recirculation in a stoichiometric, SI natural gas engine. Colorado State University, 2020.

[43] Michael Cerna and Audrey F. Harvey. The Fundamentals of Signal Analysis. 2000.

[44] Millo F, Ferraro C V. Knock in S.I. Engines: A comparison between different techniques for detection and control. SAE Technical Papers 1998;107:1091–112.

[45] Rockstroh T, Kolodziej CP, Jespersen MC, Goldsborough SS, Wallner T. Insights into Engine Knock: Comparison of Knock Metrics across Ranges of Intake Temperature and Pressure in the CFR Engine. SAE International Journal of Fuels and Lubricants 2018;11:545–62.

[46] Kar T, Zhou Z, Brear M, Yang Y, Khosravi M, Lacey J. A Comparative Study of Directly Injected, Spark Ignition Engine Combustion and Energy Transfer with Natural Gas, Gasoline and Charge Dilution. SAE International Journal of Fuels and Lubricants 2022.

[47] Pal P, Kolodziej CP, Choi S, Som S, Broatch A, Gomez-Soriano J, et al. Development of a Virtual CFR Engine Model for Knocking Combustion Analysis. SAE International Journal of Engines 2018;11:1069–82. https://doi.org/10.4271/2018-01-0187.

[48] Burgdorf K, Denbratt I. Comparison of cylinder pressure based knock detection methods. SAE Technical Papers 1997;106:1357–74. https://doi.org/10.4271/972932.

[49] Chiriac R, Radu B, Apostolescu N, Fuiorescu D. An Investigation of Knock in a Spark Ignition Engine Using LPG. SAE Technical Papers 2005;2005-Septe.

[50] Broatch A, Margot X, Novella R. Combustion noise analysis of partially premixed combustion concept using gasoline fuel in a 2-stroke engine. Energy 2016;107:612–24. https://doi.org/10.1016/j.energy.2016.04.045.

[51] ANSYS Chemkin-Pro Theory Manual. 2021.

[52] Slunecka C, Zdanowicz A, Bhoite S, Vaughan S, Olsen D, Marchese AJ. Autoignition of Premixed Liquefied Petroleum Gas in a Rapid Compression Machine : Experimental Results and Chemical Kinetic Mechanism Reduction. 12th U. S. National Combustion Meeting by the Central States Section of the Combustion Institute, vol. 2021, 2021, p. 1–10.

[53] Kar T, Fosudo T, Slunecka C, Marchese A, Windom B, Olsen D. A Study of Propane Combustion in a Spark-Ignited Cooperative Fuel Research (CFR) Engine. SAE Technical Paper Series, vol. 1, SAE International; 2022. https://doi.org/10.4271/2022-01-0404.

[54] Livengood JC, Wu PC. Correlation of autoignition phenomena in internal combustion engines and rapid compression machines. Symposium (International) on Combustion 1955;5:347–55.

[55] Khaled F, Badra J, Farooq A. Ignition delay time correlation of fuel blends based on Livengood-Wu description. Fuel 2017;209:776–86.

[56] Fagundez JLS, Sari RL, Garcia A, Pereira FM, Martins MES, Salau NPG. A chemical kinetics based investigation on laminar burning velocity and knock occurrence in a spark-ignition engine fueled with ethanol–water blends. Fuel 2020;280:118587. https://doi.org/10.1016/j.fuel.2020.118587.

[57] GT-Power : Engine Performance Application Manual. 2018.

[58] Choi, S., Kolodziej, C., Hoth, A., and Wallner, T. Development and validation of a three pressure analysis (TPA) GT-Power model of the CFR F1 / F2 engine for estimating cylinder conditions. SAE Technical 2018:1–8.

[59] Richards, K.J., Senecal, P.K., and Pomraning E. CONVERGE 3.0.18 2020.

[60] Bestel D, Bayliff S, Marchese A, Olsen D, Windom B, Xu H. Multi-Dimensional Modeling of the CFR Engine for the Investigation of SI Natural Gas Combustion and Controlled End-Gas Autoignition. ASME 2020 Internal Combustion Engine Division Fall Technical Conference 2020:1–10. https://doi.org/10.1115/icef2020-2992.

[61] Som, S., Longman, D.E., Luo, Z., Plomer M et al. Three Dimensional Simulations of Diesel Sprays Using n-Dodecane as a Surrogate. Fall Technical Meeting of the Eastern States Section of the Combustion Institute, 2011.

[62] Ewald, J. and Peters N. A Level Set Based Flamelet Model for the Prediction of Combustion in Spark Ignition Engines. 15th International Multidimensional Engine Modeling User Group, Detroit, MI: 2005.

[63] Peters N. Turbulent Combustion. Cambridge, UK: Cambridge University Press; 2000.

[64] Han Z, Reitz RD. Turbulence Modeling of Internal Combustion Engines Using RNG κ - ε Models Turbulence Modeling of Internal Combustion Engines Using RNG k-E Models 2007;2202. https://doi.org/10.1080/00102209508907782.

[65] Amsden A, O'Rourke P, Butler T. KIVA-II: A computer program for chemically reactive flows with sprays, Los Alamos - National Laboratory, report LA-11560-MS. Los Alamos National Lab (LANL) 1989:LA-11560-MS.

[66] EUROMOT. MWM MN calculation program. Https://WwwEuromotEu/Publication-and-Events/Publications/ 2019.

[67] Ramalingam A, Panigrahy S, Fenard Y, Curran H, Heufer KA. A chemical kinetic perspective on the low-temperature oxidation of propane/propene mixtures through experiments and kinetic analyses. Combustion and Flame 2021;223:361–75.

[68] Morganti KJ. A study of the knock limits of liquefied petroleum gas (LPG) in spark-ignition engines. 2013.

[69] Morganti KJ, Foong TM, Brear MJ, Da Silva G, Yang Y, Dryer FL. The research and motor octane numbers of Liquefied Petroleum Gas (LPG). Fuel 2013;108:797–811. https://doi.org/10.1016/j.fuel.2013.01.072.

[70] García A, Monsalve-Serrano J, Lago Sari R, Fogué-Robles Á, Alemahdi N, Tunér M, et al. Development of a fast-virtual CFR engine model and its use on autoignition studies. Fuel Processing Technology 2021;224. https://doi.org/10.1016/j.fuproc.2021.107031.

[71] Wei H, Feng D, Pan J, Shao A, Pan M. Knock characteristics of SI engine fueled with n-butanol in combination with different EGR rate. Energy 2017;118:190–6. https://doi.org/10.1016/j.energy.2016.11.134.

[72] Wei H, Zhu T, Shu G, Tan L, Wang Y. Gasoline engine exhaust gas recirculation - A review. Applied Energy 2012;99:534–44. https://doi.org/10.1016/j.apenergy.2012.05.011.

[73] Wei H, Feng D, Pan J, Shao A, Pan M. Knock characteristics of SI engine fueled with n-butanol in combination with different EGR rate. Energy 2017;118:190–6. https://doi.org/10.1016/j.energy.2016.11.134.

[74] Hoepke, B., Jannsen, S., Kasseris, E., and Cheng W. EGR Effects on Boosted SI Engine Operation and Knock Integral Correlation. SAE Int J Engines n.d.:547–59. https://doi.org/10.4271/2012-01-0707.

[75] Francqueville L, Michel JB. On the Effects of EGR on Spark-Ignited Gasoline Combustion at High Load. SAE International Journal of Engines 2014;7:1808–23.

[76] Zhou Z, Kar T, Yang Y, Brear M, Xu J, Lacey J, et al. Mapping K factor variations and its causes in a modern, spark-ignition engine. Fuel 2021;290:120012.

870

871

872

873 # Abbreviations

CFR	Cooperative fuel research
LPG	Liquefied petroleum gas
CR	Compression ratio
CFD	Computational fluid dynamics
SI	Spark-ignited
CAD	Crank angle degree
IMEP	Indicated mean effective pressure
LW	Livengood-Wu
3D	Three dimensional
FFT	Fast Fourier Transform
KL	Knock integral
MAPO	Maximum amplitude of pressure oscillation
PP	Peak pressure
PSD	Power spectral density
IDT	Ignition delay time
TPA	Three pressure analysis
RANS	Reynolds-averaged Navier-Stoke
aTDC	After top dead center
MN	Methane number
P-T	Pressure-temperature
RON	Research octane number
MON	Motor octane number

AHRR	Apparent heat release rate

Symbols

γ	Ratio of specific heats
τ_{ign}	Time delay until ignition
τ	Instantaneous ignition delay time
S_t	Turbulent flame sped
S_l	Laminar flame speed
u`	Turbulent velocity fluctuation
$\dot{m}_{EGR}$	EGR mass flow rate
$\dot{m}_{total}$	Total mass flow rate